Dewetting of Silica Surfaces upon Reactions with Supercritical CO_2 and Brine: Pore-Scale Studies in Micromodels

Yongman Kim, Jiamin Wan, Timothy J. Kneafsey, Tetsu K. Tokunaga*

Earth Sciences Division, Lawrence Berkeley National Laboratory,

1 Cyclotron Road, Berkeley, California 94720, USA

* Corresponding author. Phone: 1-510-486-6004. Fax: 1-510-486-7152. Email: jwan@lbl.gov

ABSTRACT

Wettability of reservoir minerals and rocks is a critical factor controlling CO_2 mobility, residual trapping and safe-storage in geologic carbon sequestration, and currently is the factor imparting the greatest uncertainty in predicting capillary behavior in porous media. Very little information on wettability in supercritical CO_2 ($scCO_2$)-mineral-brine systems is available. We studied pore-scale wettability and wettability alteration in $scCO_2$-silica-brine systems using engineered micromodels (transparent pore networks), at 8.5 MPa and 45 °C, over a wide range of NaCl concentrations up to 5.0 M. Dewetting of silica surfaces upon reactions with $scCO_2$ was observed through water film thinning, water droplet formation, and contact angle increases within single pores. The brine contact angles increased from initial values near 0˚ up to 80˚ with larger increases under higher ionic strength conditions. Given the abundance of silica surfaces in reservoirs and caprocks, these results indicate that CO_2 induced dewetting may have important consequences on CO_2 sequestration including reducing capillary entry pressure, and altering quantities of CO_2 residual trapping, relative permeability, and caprock integrity.

KEYWORDS

dewetting, wettability, supercritical CO_2, micromodel, pore-scale wettability, contact angle, water film thinning, capillary pressure.

1. Introduction

Geological CO_2 storage is one of the most promising methods to reduce anthropogenic CO_2 emissions into the atmosphere. Candidate geologic CO_2 storage sites are mainly deep saline aquifers, depleted oil and gas reservoirs, unmineable coal seams, and deep ocean sediments [1, 2]. Because of its lower density relative to water, containment of CO_2 within reservoirs requires prevention of its buoyant entry into and escape through overlying caprock (seal) formations. Wettability of reservoir rocks strongly influences CO_2 flow and distribution, and quantities of residual CO_2 trapping [3, 4]. Wettability of caprocks directly impacts the maximum injection pressure and storage height [5, 6] through altering the capillary breakthrough pressure. The capillary breakthrough pressure ($P_{c,CO2}$) is the excess CO_2 phase pressure (relative to the brine phase) required to initiate CO_2 flow through geologic medium previously saturated with brine. Capillary breakthrough pressure of CO_2 can be estimated with the Young-Laplace equation.

$$P_{c,CO_2} = \frac{2\gamma_{w,CO_2}\cos\theta}{r} \quad (1)$$

where $\gamma_{w,CO2}$ is the interfacial tension (IFT) between CO_2 and the aqueous phase, θ is the contact angle of the aqueous phase on the mineral surface, and r is the characteristic radius of the pores controlling percolation of CO_2. The range of r is a local property of the geologic material, typically ranging from a few to hundreds of μm in reservoirs, and in the nm range for caprocks. Values of $\gamma_{w,CO2}$ are relatively well constrained, being between 20 to 35 mN m^{-1} under the pressures, temperatures, and salinities associated with $scCO_2$ sequestration [5, 7-10]. Variations in θ have large consequences because increases toward 90˚ and greater lead to diminishing of $P_{c,CO2}$ and even its reversal, allowing spontaneous imbibition of CO_2 in absence of excess pressure. Measurements of θ are commonly obtained on macroscopic surfaces with droplet sizes typically in the range of a few mm. Wettability is also inferred from macroscopic measurements

of capillary displacement (core flooding) of immiscible fluids. However, direct measurement of wettability within porous media remains challenging. Therefore wettability is currently the factor imparting the greatest uncertainty in predicting capillary behavior in porous media.

Injected CO_2 is usually assumed to behave as a non-wetting fluid in geological formations (water-wet). However, this assumption was recently questioned, and partial wetting of CO_2 on mineral surfaces has been investigated by several groups [8, 11-16]. Although wettability change has significant implications, there is still a paucity of data addressing this phenomenon under geological CO_2 storage conditions, particularly at the pore-scale.

Silica-CO_2 interactions have been studied through laboratory experiments [17-24]. and molecular simulations [20, 25, 26]. For example, Dickson *et al*. investigated contact angle changes when CO_2 reacts with silanol groups on the modified silica surfaces [19]. Tripp and Combes showed that CO_2 removes water from silica surfaces more effectively than organic solvents [21]. McCool and Tripp reported that the reacted $scCO_2$ with silica hydroxyls could not be removed from the silica surface by simple evacuation [22]. Cole *et al.* studied the interaction of $scCO_2$ in nanoscale pores of shale and reported that $scCO_2$ may interact with muscovite hydroxyl groups resulting in significant decrease of its mobility [20]. Vishnyakov *et al*. studied the interactions between $scCO_2$ and silica nanoparticles using molecular simulations, and reported that $scCO_2$ strongly reacts with hydroxyl groups on the silica surface via hydrogen bonds [25]. Complications in contact angle measurements associated with potential surface contamination can add significant uncertainty [27, 28]. These findings indicate that $scCO_2$ may alter the wettability of silica surface, and also that $scCO_2$ becomes the partially wetting phase as pressure increases. However, these previous studies did not provide direct evidence of wettability changes within pores.

Micromodels are transparent pore networks used for laboratory studies of microscopic distribution and transport of fluids in porous media [29] in many different applications including research related to oil recovery from reservoirs [30-32], nonaqueous phase liquid dissolution [33-36], and colloid transport [37-42]. Few micromodel experiments have been conducted under elevated pressure and temperature [8, 30, 43-50], and even fewer have been conducted under supercritical CO_2 conditions. Chalbaud *et al*. investigated distributions of CO_2 and water in glass micromodels having different wettabilities [8]. Zhang *et al*. studied CO_2 and water displacement in a micromodel with dual-permeability pore size distributions [46]. Riazi *et al*. observed displacement behavior indicating that CO_2 injected into depleted oil reservoirs may have faster breakthrough relative to injection into aquifers of similar pore geometry [47]. Er *et al*. visually analyzed CO_2 and oil interactions near the fracture region inside a micromodel matrix [49]. Despite their versatility, limitations common to most micromodels include intrinsic restriction to two-dimensional pore networks of uniform etch depth, relatively uniform surface chemistry (silica glasses or organic polymers), relatively smooth surface microtopography, and lack of pore sizes finer than about 10 μm. To the best of our knowledge, quantitative studies addressing wettability alteration at the pore-scale under supercritical CO_2 conditions have yet to be reported.

The objective of this study is to understand if, and to what extent, interactions with $scCO_2$ change the wettability of silica, the most common reservoir solid. We utilized transparent engineered silica micromodels to study the wetting behavior of $scCO_2$ through direct visualization of the phase displacement processes, and measurement of contact angle alterations, at the pore-scale under conditions relevant to geological CO_2 storage.

2. Method

2.1. Micromodel.

The high-pressure micromodels used in this study were fabricated by Micronit Microfluidics BV. These were made out of fused silica plates (Schott Lithotec, Lithosil^{TM} Q1), with homogenous pore network patterns etched on the fused silica plates with hydrofluoric acid. Two symmetrically patterned plates were fused together to form a homogeneous 2-dimensional porous network having a patterned area of 20 mm x 10 mm, composed of 576 discoid silica grains (590 μm diameter). Two different homogenous patterns were used for the current work, with pore volumes (PV) of 0.31 and 0.89 μL (pattern parameters described in supporting information (SI)). The top (plan view) and cross-section images of the micromodel are shown in Fig. 1. A unique feature of the micromodel pattern is that the grains do not contact with each other (unlike the real porous media). This design minimizes accumulation of residual water in pendular structures between grains, and allowed clearer observations of water layer and wettability changes and contact angle measurements.

2.2. High pressure microscopy/micromodel system.

An inverted microscope (Carl Zeiss, Observer Z1.m) was used for viewing, with images recorded using a CCD camera (Carl Zeiss, AxioCam MRc5) connected to a computer. The micromodel was placed horizontally on the customer-designed stage of the microscope. Brine (without pre-reacting with CO_2) was filled into the micromodel using a stainless steel syringe (KD scientific, 2.5 mL with 1/16" Swagelok^{TM} fitting) controlled with a precision syringe pump (Harvard, PHD 2000). A precision, high-pressure syringe pump (Teledyne ISCO, 500HP) was used to fill $scCO_2$ (pre-saturated with water) into the micromodel. To prepare $scCO_2$, a

commercial CO_2 cylinder (Airgas, 99.99%) equipped with an eductor tube was connected to the ISCO pump. The prepared $scCO_2$ was pre-saturated with water at 8.5 MPa 45 °C in a stirred reactor (Parr, Model 4560). Pressure was measured with a pressure transducer (Omega, PXM01MD0-400BARGV). The system was contained in an insulated enclosure, heated with a forced convection heater and heating tape, controlled with PID controllers (Cole Parmer, EW-89000-10) connected to thermocouples (Omega, Type T). Additional description of the experimental system and a schematic diagram are provided in SI.

2.3. Experiment Procedures.

Sodium chloride brines (0.01 to 5.00 M) were prepared with deionized (DI) water (Barnstead, NanoPure) and NaCl (Sigma-Aldrich, ACS reagent grade). The pH values of the brines were between 5.8 and 6.2 depending on ionic strength. Brines were degassed and stored at room temperature under vacuum until being used. A micromodel was cleaned before usage by injecting 5 mL of absolute ethanol (Mallinckodt Baker, ACS reagent grade) followed by 20 mL of DI water. Then it was dried at 120 °C for 24 h in a drying oven. After the clean micromodel was assembled in the experimental system, vacuum was applied for 3 h at 45 °C in order to remove residual air inside the micromodel and the flow lines. All components directly connected with the micromodel were kept inside the thermal insulation chamber (SI, Figure S1) to maintain a temperature of 45 ±1 °C during experiments. Degassed brine was then injected into the micromodel until the flow lines and the micromodel were fully saturated. The system was then gradually pressurized with the syringe pumps up to 8.5 MPa over a period of 30 min. So far the prepared $scCO_2$ was kept isolated from the brine. In order for the $scCO_2$ and the brine to reach thermal equilibrium, the system was equilibrated at 45 °C for 3 h, then the brine drainage process

($scCO_2$ invasion) was initiated. The syringe pump on the brine side (Harvard) withdrew brine at a constant flow rate (4 μL min^{-1} for 20 min), and the pump on the $scCO_2$ side (ISCO) injected the $scCO_2$ at constant pressure. A total 90 PV of $scCO_2$ was injected during the brine drainage process. Upon completion of the drainage the inlet and outlet of the micromodel were closed off, and the system was then equilibrated at the same pressure and temperature. Images of $scCO_2$ and brine distributions in the micromodel were recorded through and after the drainage process.

In order to isolate the effects caused by surface reactions with CO_2, an experiment using air as the non-wetting fluid was conducted at atmospheric pressure. The micromodel was saturated with DI water and then air was injected at 8 μL min^{-1} for 15 min under ambient pressure and temperature. Images of fluid phase distributions in the water-air system were record using the same method described above.

2.4. Image analyses.

ImageJ software [51] combined with a contact angle plug-in (Marco Brugnara, marco.brugnara@ing.unitn.it) was used to analyze the acquired images. The shape of the silica grains on the imaging plane is circular, thus contact lines of the brine droplets are curved rather than flat. Therefore the curved wetting surface must be accounted for when determining intrinsic contact angles (the equivalent angle expected if the brine droplet is deposited on a flat surface of the same composition). Details of the analysis procedure and discussion about contact angles on curved surfaces can be found in the work of Extrand and Moon [52] and Marmur and Krasovitski [53]. Some example images of the contact angle measurement process with ImageJ are shown in the SI.

3. Results and Discussion

3.1. Air as the non-aqueous phase: the control experiment

This experiment was conducted to understand the wetting behavior of the silica pore walls of the micromodels when air is the non-aqueous phase. The experimental procedures and conditions were the same as those used with CO_2 as the non-aqueous phase, except that the total pressure was 0.1 MPa. Representative images taken at the end of the water drainage (air displaced water in the pore spaces) are shown in Figure 2. After drainage, the residual water remained as thick films between the silica grains and air. In order to visually record the existence of water films, we imposed a steady flow of air to impart shear stress at air-water interfaces. The airflow pushed the water films to form accumulate as bulges along the downstream sides of the silica grains, with advancing contact angles of 11.5˚ ±1.6°. Upon stopping airflow, the water bulges retracted back into thick water films with static contact angles near 0°. This demonstrated that the silica micromodel is strongly hydrophilic when air is the non-aqueous phase.

3.2. $scCO_2$ as the non-aqueous phase

Figure 3 shows representative images taken during the drainage of 1 M NaCl brine displaced by $scCO_2$ at 8.5 MPa and 45 °C. The micromodel was set vertically and the $scCO_2$ was injected from the bottom to the top at the rate of 4 μL/min for 20 min. These images were taken directly by using a digital camera (Nikon D90, 12.3 Megapixel) in order to view the entire pore network of the micromodel, instead of using the CCD camera through the microscope (for individual pores). The photographs show how the scCO2 flow paths developed over time, and the time-dependent saturation distributions. The phase saturation can be quantitatively determined from the images, and many other studies can be done using this method. Although gravity influences

flow paths and the spatial distribution of phases, it does not affect surface wetting properties that are of primary interest in this study.

During and after the drainage ($scCO_2$ injection) process described in the previous paragraph, we observed dewetting of silica surfaces through water-film thinning, formation and growth of water droplets, and contact angle increase. Figure 4 shows the water droplets formed during and after the drainage. The photographs were taken 2 h after initiating the drainage process, when the droplet sizes, shapes, and contact angles had reached apparent steady state (based on analyzing the continuous video recording). The measured equilibrium contact angles ranged from 40˚ to 80˚. The originally water-wet (Figure 2) silica grains now became intermediate wet through $scCO_2$ reactions with the silica surfaces in brine. Immediately after drainage ($scCO_2$ displaced brine), the residual water was initially retained as thick and smooth films coating on the silica surfaces (pore walls). As the $scCO_2$ reacted with silica, surfaces became less hydrophilic, allowing the residual water films to thin through surface tension driven redistribution into local droplets seen in Figure 4. In 3-dimensional porous media, the dewetting would drive the excess water into pendular rings among grain-grain contacts, and into local microtopographic minima along rough grain surfaces.

3.3. Time dependence of contact angles change

Upon displacement of brine by $scCO_2$, changes of residual water configuration on silica grain surfaces were observed only over a short time period. Images of water droplet growth during the drainage process with 0.01 M NaCl are shown in Figure 5. The image capture rate for the microscope camera was 0.45 s $frame^{-1}$, and a small field of view was monitored for 2 h. Water droplet growth was only observed over about a 20 s period during monitoring. This may be

mainly because of the narrow monitoring field of view (locations of droplet growth cannot be predicted and preselected for monitoring). In Figure 5, the '0 sec' image was captured 1 s prior to the image showing appreciable water droplet growth. Times shown in other images are relative to '0 sec'. While the size of the brine droplets gradually increased over the time, the apparent contact angle did not change significantly after the observed initial droplet formation. Apparently, most of the dewetting occurred quickly after $scCO_2$ entered pores, within the timeframe of seconds.

3.4. Effect of ionic strength.

To understand effects of ionic strength on wetting behavior of the $scCO_2$-brine-silica system, ionic strength of brine was varied from 0.01 to 5 M NaCl. Figure 6 shows the effect of ionic strength on wettability at equilibrium following brine drainage. The darker areas between the circular grains are water droplets and the brighter areas are $scCO_2$. Note that the lines between the brine droplets and the silica grains are thinner than between $scCO_2$ and silica grains, because of the different refractive indices (RI) of the different materials. The reported RI of the fused silica is 1.458 (provided by the manufacturer), brine 1.391 [54], and $scCO_2$ under our experimental pressure and temperature is 1.088 [55]. The RI difference between the water and the silica is smaller than that between $scCO_2$ and silica. Some example images of the contact angle measurement process using ImageJ software are shown in Figure S2 of the SI. The measured contact angles are in the range of 50˚ to 75˚ (mean value = 66.4˚) for 1 M NaCl, 55˚ to 76˚ (mean value = 65.4˚) for 3 M NaCl, and 66˚ to 87˚ (mean value = 75.1˚) for 5 M NaCl. Contact angles for the 0.01 M NaCl condition are not reported here because values for the majority of the water droplets were too low to be determined by image analysis. However, it is

worth mentioning that a few droplets had contact angles over 60° in 0.01 M NaCl, suggesting that even in this otherwise homogeneous system, variability in local wettability can be significant. The trend is clear that water wettability of silica surfaces decreases with increased brine salt concentrations in the $scCO_2$-brine-silica system.

3.5. Non-axisymmetric brine-droplets

Unlike conventional methods (e.g., sessile drop) for measuring contact angle, the droplets in micromodels are not axisymmetric. In micromodels the observed radius of curvature R_1 of any point along a droplet interface has its associated second principal radius R_2 on a plane orthogonal to the focal plane. Although this second principal radius cannot be imaged with conventional optical microscopy, it can be calculated. We assume that the contact angle θ measured on the microscope focal plane is equal to the contact angle in planes transecting observed radii of curvature and orthogonal to the view plane. If the pore depth d_2 is known, the associated pore radius r_2 is simply half the pore depth, such that the second radius of curvature $R_2 = d/(2\cos\theta)$. The differential (capillary) pressure in the droplet relative to the nonwetting phase can then be calculated with the Young-Laplace equation expressed as

$$\Delta P = \gamma_{w,CO2}\left(\frac{1}{R_1} + \frac{2\cos\theta}{d}\right) \tag{2}$$

Assuming local equilibrium between the capillary and adsorbed water [56, 57], equation (2) can be used to estimate lower magnitudes of disjoining pressures [58, 59] in residual water films. The magnitude of ΔP in our systems ranged up to about 10 kPa, with larger values associated

with smaller R_1 and small θ. Equation (2) also indicates that droplets with different combinations of θ and R_1 can be in capillary pressure disequilibrium.

3.6. Mechanisms responsible for dewetting

The ability of water to remain attached to a mineral surface (wettability) results from intermolecular interactions among the three phases; the mineral, aqueous and non-aqueous fluids. The main chemical groups on silica surfaces in aqueous solutions are silanol and silicilic acid groups [60]. The hydrophilicity of silica depends on the surface density of these functional groups. At near neutral pH, some silica surfaces are negatively charged through deprotonation of silanol sites as in Reaction (1) below. The measured pK_a values for Reaction (1) are in the range of 5.7 and 7.7 [61]. When $scCO_2$ dissolves into brine, the brine pH becomes about 3.0 [62]. Thus Reactions (1) shift to the left, and the surface charge of silica is diminished.

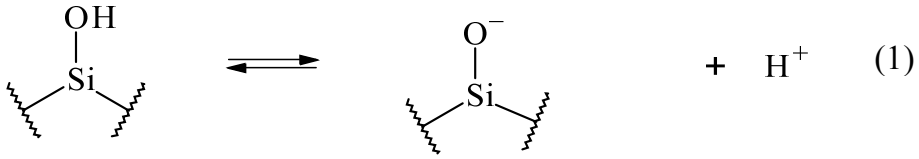

(1)

The pH effect on silica wettability reported by Gribanova was that when pH is decreased from 6 to 3, contact angle increased from 19° to 23° in the air-brine-silica system at ambient pressure and temperature [63]. Chiquet *et al*. explained that the decreased surface charge with decreased pH results in destabilizing the water film, therefore increases contact angles [11]. Other factors besides pH-dependent surface charge may also contribute to explain the magnitude of the measured wettability changes through reaction with $scCO_2$. Recently, Puah *et al*. studied the effect of surface charge on wettability and wetting kinetics by measuring contact angles on a coated titania surface [64]. They analyzed the experimental results using molecular-kinetic

theory and concluded that surface charge affects both the static and dynamic wettability. Dickson *et al*. proposed that the reaction between CO_2 and the silanol group is physical adsorption capping the silanol groups providing an additional mechanism to explain the increased contact angle [19]. Vishnyakov *et al*. reported that $scCO_2$ can strongly react with hydroxyl groups on silica substrates via hydrogen bonds [25]. The electric double layer within high ionic strength films on acidic silica surfaces is predicted to become highly compressed because of the very low surface charge density being balanced over short (nm) distances (Tokunaga 2011) [65]. Although research on mechanisms responsible for wettability change in systems like ours is ongoing, it is clear that reactions with $scCO_2$ reduce the wettability of silica surfaces.

As shown in the pore cross-section in Fig. 1(c), pore "depth" is much less than their widths. Upon CO_2 entry, capillarity will stabilize the wetting brine phase along the rounded pore "edges" at the grain surfaces in the micromodel. Minimization of capillary interfacial area will favor stabilization of pendular rings between grains and droplets along grain surfaces, rather than allowing persistence of uniformly thick water films on all surfaces. As the silica reacted with $scCO_2$, its surfaces became less water wettable, resulting in water film thinning and surface tension driven water redistributing into droplets along pore edges. This dewetting process is depicted in Figure S3 in SI.

We also observed increased contact angles as brine salinity increases, consistent with Sghaier et al. [66], who found increased contact angle with increased NaCl concentration on hydrophilic surfaces. Ion exclusion at water-fluid interfaces with increased salinity [67-70] increases the $scCO_2$/brine IFT [7, 8] and contributes to contact angle increases. The reduced film thickness from compression of the electric double layer may permit greater $scCO_2$ reaction with silica, resulting in decreased energy of its surface. If the IFT of brine/silica and of $scCO_2$/silica

are independent of salinity (or the dependence is negligible), then the contact angle increase may largely correspond to the increased IFT of $scCO_2$/brine. However, quantitative relations between the IFTs and contact angles in various brine concentrations have not yet been reported [11, 71]. Our investigation on contact angle salinity dependence in $scCO_2$-brine-mineral systems is in progress.

4. Implications

In reservoirs used for geological CO_2 sequestration, the injected CO_2 will inevitably interact with reservoir minerals. The present work provides an improved understanding on the wetting behavior of CO_2 under deep reservoir conditions, showing that CO_2 cannot be treated as a simple non-wetting fluid in reservoir pores. Supercritical CO_2 can react quickly (within seconds) with silica resulting in dewetting of the silica surface. The process of dewetting, water-film thinning, water droplet formation, and contact angle increase were visualized in our micromodels. The contact angle on silica increased from the initial near 0˚ up to 80˚, depending on ionic strength. The higher ionic strength results in larger contact angles. Given the abundance of silica surfaces in the subsurface, these results imply that CO_2 injection-induced dewetting may have important consequences on CO_2 sequestration, including determining CO_2 residual saturation (a major trapping mechanism), CO_2 flow paths and relative permeability (mobility), and capillary entry pressure (injectivity and caprock integrity). We do not yet know if the dewetting phenomenon observed on silica also occurs on other mineral surfaces. Although two-dimensional micromodels have their limitations as representations of natural porous medium, they permit the spatial and temporal resolution required for investigating critical pore scale phenomena such as wettability and capillary entry.

Acknowledgements

The authors sincerely thank the four anonymous reviews and associate editor Dr. Dzombak for their insightful and constructive comments and suggestions. This material is based upon work supported as part of the Center for Nanoscale Control of Geologic CO2, an Energy Frontier Research Center funded by the U.S. Department of Energy, Office of Science, Office of Basic Energy Sciences under Award Number DE-AC02-05CH11231.

REFERENCES

1. Intergovernmental Panel on Climate Change. Working Group III., *IPCC special report on carbon dioxide capture and storage*. Cambridge University Press, for the Intergovernmental Panel on Climate Change: Cambridge, 2005; p x, 431 p.
2. Shukla, R.; Ranjith, P.; Haque, A.; Choi, X., A review of studies on CO_2 sequestration and caprock integrity. *Fuel* **2010,** *89*, (10), 2651-2664.
3. Saadatpoor, E.; Bryant, S. L.; Sepehrnoori, K., New Trapping Mechanism in Carbon Sequestration. *Transp. Porous Media* **2010,** *82*, (1), 3-17.
4. Krevor, S. C. M.; Pini, R.; Li, B. X.; Benson, S. M., Capillary heterogeneity trapping of CO_2 in a sandstone rock at reservoir conditions. *Geophys. Res. Lett.* **2011,** *38*.
5. Li, Z. W.; Dong, M. Z.; Li, S. L.; Huang, S., CO_2 sequestration in depleted oil and gas reservoirs - caprock characterization and storage capacity. *Energ Convers Manage* **2006,** *47*, (11-12), 1372-1382.
6. Naylor, M.; Wilkinson, M.; Haszeldine, R. S., Calculation of CO_2 column heights in depleted gas fields from known pre-production gas column heights. *Mar Petrol Geol* **2011,** *28*, (5), 1083-1093.
7. Bachu, S.; Bennion, D. B., Interfacial Tension between CO_2, Freshwater, and Brine in the Range of Pressure from (2 to 27) MPa, Temperature from (20 to 125) degrees C, and Water Salinity from (0 to 334 000) mg(.)L(-1). *J Chem Eng Data* **2009,** *54*, (3), 765-775.
8. Chalbaud, C.; Robin, M.; Lombard, J. M.; Martin, F.; Egermann, P.; Bertin, H., Interfacial tension measurements and wettability evaluation for geological CO_2 storage. *Adv Water Resour* **2009,** *32*, (1), 98-109.

9. Chiquet, P.; Daridon, J. L.; Broseta, D.; Thibeau, S., CO_2/water interfacial tensions under pressure and temperature conditions of CO_2 geological storage. *Energ Convers Manage* **2007,** *48*, (3), 736-744.
10. Schulz, C.; Jaeger, P. T.; Eggers, R. In *Wettability of reservoir rock materials in high pressure carbon dioxide*, The 11th International Symposium on Reservoir Wettability, University of Calgary, AB, Canada, September 6-9, 2010; University of Calgary, AB, Canada, 2010.
11. Chiquet, P.; Broseta, D.; Thibeau, S., Wettability alteration of caprock minerals by carbon dioxide. *Geofluids* **2007,** *7*, (2), 112-122.
12. Yang, D. Y.; Gu, Y. G.; Tontiwachwuthikul, P., Wettability determination of the reservoir brine-reservoir rock system with dissolution of CO_2 at high pressures and elevated temperatures. *Energ Fuel* **2008,** *22*, (1), 504-509.
13. Siemons, N.; Bruining, H.; Castelijns, H.; Wolf, K. H., Pressure dependence of the contact angle in a CO_2-H_2O-coal system. *J Colloid Interf Sci* **2006,** *297*, (2), 755-761.
14. Espinoza, D. N.; Santamarina, J. C., Water-CO_2-mineral systems: Interfacial tension, contact angle, and diffusion-Implications to CO_2 geological storage. *Water Resour Res* **2010,** *46*, W07537.
15. Jaeger, P. T.; Alotaibi, M. B.; Nasr-El-Din, H. A., Influence of Compressed Carbon Dioxide on the Capillarity of the Gas-Crude Oil-Reservoir Water System. *J Chem Eng Data* **2010,** *55*, (11), 5246-5251.
16. Hildenbrand, A.; Schlomer, S.; Krooss, B. M.; Littke, R., Gas breakthrough experiments on pelitic rocks: comparative study with N_2, CO_2 and CH_4. *Geofluids* **2004,** *4*, (1), 61-80.
17. Di Giovanni, O.; Dorfler, W.; Mazzotti, M.; Morbidelli, M., Adsorption of supercritical carbon dioxide on silica. *Langmuir* **2001,** *17*, (14), 4316-4321.
18. Roque-Malherbe, R.; Polanco-Estrella, R.; Marquez-Linares, F., Study of the Interaction between Silica Surfaces and the Carbon Dioxide Molecule. *J Phys Chem C* **2010,** *114*, (41), 17773-17787.
19. Dickson, J. L.; Gupta, G.; Horozov, T. S.; Binks, B. P.; Johnston, K. P., Wetting phenomena at the CO_2/Water/Glass interface. *Langmuir* **2006,** *22*, 2161-2170.
20. Cole, D. R.; Chialvo, A. A.; Rother, G.; Vlcek, L.; Cummings, P. T., Supercritical fluid behavior at nanoscale interfaces: Implications for CO_2 sequestration in geologic formations. *Philos Mag* **2010,** *90*, (17-18), 2339-2363.
21. Tripp, C. P.; Combes, J. R., Chemical modification of metal oxide surfaces in supercritical CO_2: The interaction of supercritical CO_2 with the adsorbed water layer and the surface hydroxyl groups of a silica surface. *Langmuir* **1998,** *14*, (26), 7350-7352.
22. McCool, B.; Tripp, C. P., Inaccessible hydroxyl groups on silica are accessible in supercritical CO_2. *J Phys Chem B* **2005,** *109*, (18), 8914-8919.
23. Dickson, J. L.; Binks, B. P.; Johnston, K. P., Stabilization of carbon dioxide-in-water emulsions with silica nanoparticles. *Langmuir* **2004,** *20*, (19), 7976-7983.
24. Bikkina, P. K., Contact angle measurements of CO_2-water-quartz/calcite systems in the perspective of carbon sequestration. *International Journal of Greenhouse Gas Control* **2011,** *5*, 1259-1271.
25. Vishnyakov, A.; Shen, Y. Y.; Tomassone, M. S., Interactions of silica nanoparticles in supercritical carbon dioxide. *J Chem Phys* **2008,** *129*, (17), 174704.
26. Liu, S. Y.; Yang, X. N.; Yan, Q., Molecular dynamics simulation of wetting behavior at CO_2/water/solid interfaces. *Chinese Sci Bull* **2010,** *55*, (21), 2252-2257.

27. Mahadevan, J., Comments on the paper titled "Contact angle measurements of CO2-water-quartz/calcite systems in the perspective of carbon sequestration": A case of contamination? *International Journal of Greenhouse Gas Control* **2011**.
28. Bikkina, P. K., Reply to the comments on "Contact angle measurements of CO2-water-quartz/calcite systems in the perspective of carbon sequestration. *International Journal of Greenhouse Gas Control* **2011**.
29. Wan, J. M.; Tokunaga, T. K.; Tsang, C. F.; Bodvarsson, G. S., Improved glass micromodel methods for studies of flow and transport in fractured porous media. *Water Resour Res* **1996,** *32*, (7), 1955-1964.
30. Sohrabi, M.; Danesh, A.; Jamiolahmady, M., Visualisation of residual oil recovery by near-miscible gas and SWAG injection using high-pressure micromodels. *Transp. Porous Media* **2008,** *74*, (2), 239-257.
31. Mohammadzadeh, O.; Rezaei, N.; Chatzis, I., Pore-Level Investigation of Heavy Oil and Bitumen Recovery Using Solvent -Aided Steam Assisted Gravity Drainage (SA-SAGD) Process. *Energ Fuel* **2010,** *24*, 6327-6345.
32. Hatiboglu, C. U.; Babadagli, T., Pore-scale studies of spontaneous imbibition into oil-saturated porous media. *Phys Rev E* **2008,** *77*, (6), 066311.
33. Sharmin, R.; Ioannidis, M. A.; Legge, R. L., Effect of nonionic surfactant partitioning on the dissolution kinetics of residual perchloroethylene in a model porous medium. *J Contam Hydrol* **2006,** *82*, (1-2), 145-164.
34. Sahloul, N. A.; Ioannidis, M. A.; Chatzis, I., Dissolution of residual non-aqueous phase liquids in porous media: pore-scale mechanisms and mass transfer rates. *Adv Water Resour* **2002,** *25*, (1), 33-49.
35. Zhong, L. R.; Mayer, A.; Glass, R. J., Visualization of surfactant-enhanced nonaqueous phase liquid mobilization and solubilization in a two-dimensional micromodel. *Water Resour Res* **2001,** *37*, (3), 523-537.
36. Fenwick, D. H.; Blunt, M. J., Three-dimensional modeling of three phase imbibition and drainage. *Adv Water Resour* **1998,** *21*, (2), 121-143.
37. Wan, J. M.; Wilson, J. L., Visualization of the role of the gas-water interface on the fate and transport of collids in porous-media. *Water Resour Res* **1994,** *30*, (1), 11-23.
38. Wan, J. M.; Wilson, J. L.; Kieft, T. L., Influence of the gas-water interface on transport of microorganisms through unsaturated porous-media. *Appl. Environ. Microbiol.* **1994,** *60*, (2), 509-516.
39. Wan, J. M.; Wilson, J. L., Colloid transport in unsaturated porous-media. *Water Resour Res* **1994,** *30*, (4), 857-864.
40. Guzman, K. A. D.; Finnegan, M. P.; Banfield, J. F., Influence of surface potential on aggregation and transport of titania nanoparticles. *Environ. Sci. Technol.* **2006,** *40*, (24), 7688-7693.
41. Baumann, T.; Toops, L.; Niessner, R., Colloid dispersion on the pore scale. *Water Res.* **2010,** *44*, (4), 1246-1254.
42. Auset, M.; Keller, A. A., Pore-scale visualization of colloid straining and filtration in saturated porous media using micromodels. *Water Resour Res* **2006,** *42*, (12), W12S02.
43. Grate, J. W.; Zhang, C. Y.; Wietsma, T. W.; Warner, M. G.; Anheier, N. C.; Bernacki, B. E.; Orr, G.; Oostrom, M., A note on the visualization of wetting film structures and a nonwetting immiscible fluid in a pore network micromodel using a solvatochromic dye. *Water Resour Res* **2010,** *46*, W1602.

44. Riazi, M.; Sohrabi, M.; Jamiolahmady, M., Experimental Study of Pore-Scale Mechanisms of Carbonated Water Injection. *Transp. Porous Media* **2011,** *86*, (1), 73-86.
45. Wu, X.; Zhao, R.; Wang, R., Visual Experimental Study of the Factors Affecting the Stability of Foamy Oil Flow. *Pet. Sci. Technol.* **2011,** *29*, (14), 1449-1458.
46. Zhang, C.; Oostrom, M.; Grate, J. W.; Wietsma, T. W.; Warner, M. G., Liquid CO2 Displacement of Water in a Dual-Permeability Pore Network Micromodel. *Environ. Sci. Technol.* **2011,** *45*, (17), 7581-8.
47. Riazi, M.; Sohrabi, M.; Bernstone, C.; Jamiolahmady, M.; Ireland, S., Visualization of mechanisms involved in CO_2 injection and storage in hydrocarbon reservoirs and water-bearing aquifers. *Chemical Engineering Research and Design* **2011,** *89*, 1827-1840.
48. Dawe, R. A.; Caruana, A.; Grattoni, C. A., Immiscible Displacement in Cross-Bedded Heterogeneous Porous Media. *Transp. Porous Media* **2011,** *87*, (1), 335-353.
49. Er, V.; Babadagli, T.; Xu, Z. H., Pore-Scale Investigation of the Matrix-Fracture Interaction During CO_2 Injection in Naturally Fractured Oil Reservoirs. *Energ Fuel* **2010,** *24*, 1421-1430.
50. Rangel-German, E. R.; Kovscek, A. R., A micromodel investigation of two-phase matrix-fracture transfer mechanisms. *Water Resour Res* **2006,** *42*, (3), W03401.
51. Abramoff, M. D.; Magalhaes, P. J.; Ram, S. J., Image Processing with ImageJ. *Biophotonics International* **2004,** *11*, (7), 36-42.
52. Extrand, C. W.; Moon, S. I., Contact angles on spherical surfaces. *Langmuir* **2008,** *24*, (17), 9470-9473.
53. Marmur, A.; Krasovitski, B., Line tension on curved surfaces: Liquid drops on solid micro- and nanospheres. *Langmuir* **2002,** *18*, (23), 8919-8923.
54. Schiebener, P.; Straub, J.; Sengers, J.; Gallagher, J. S., Refractive-index of water and steam as function of wavelength, temperature and density. *J. Phys. Chem. Ref. Data* **1990,** *19*, (3), 677-717.
55. Sun, Y. D.; Shekunov, B. Y.; York, P., Refractive index of supercritical CO_2-ethanol solvents. *Chemical Engineering Communications* **2003,** *190*, (1), 1-14.
56. Langmuir, I., Repulsive forces between charged surfaces in water, and the cause of the Jones-Ray effect. *Science* **1938,** *88*, 430-432.
57. Buckingham, E. *Studies on the movement of soil moisture*; Bureau of Soils, U. S. Department Agriculture, Government Printing Office, Washington, DC: 1907.
58. Hirasaki, G. J., Wettability: Fundamentals and surface forces. *SPE Formation Evaluation* **1991,** *June 1991*, 217-226.
59. Israelachvili, J. N., *Intermolecular and Surfaces Forces*. 2nd ed.; Academic Press: London, 1991; p 450.
60. Vigil, G.; Xu, Z. H.; Steinberg, S.; Israelachvili, J., Interactions of Silica Surfaces. *J Colloid Interf Sci* **1994,** *165*, (2), 367-385.
61. Dove, P. M.; Craven, C. M., Surface charge density on silica in alkali and alkaline earth chloride electrolyte solutions. *Geochimica Et Cosmochimica Acta* **2005,** *69*, (21), 4963-4970.
62. Kaszuba, J. P.; Janecky, D. R.; Snow, M. G., Carbon dioxide reaction processes in a model brine aquifer at 200 degrees C and 200 bars: implications for geologic sequestration of carbon. *Appl. Geochem.* **2003,** *18*, (7), 1065-1080.
63. Gribanova, E. V., Dynamic Contact Angles - Temperature-Dependence and the Influence of the State of the Adsorption Film. *Adv Colloid Interfac* **1992,** *39*, 235-255.

64. Puah, L. S.; Sedev, R.; Fornasiero, D.; Ralston, J., Influence of Surface Charge on Wetting Kinetics. *Langmuir* **2010,** *26*, (22), 17218-17224.
65. Tokunaga, T. K., Physicochemical controls on adsorbed water film thickness in unsaturated geological media. *Water Resour. Res.* **2011,** *47*, W08514.
66. Sghaier, N.; Prat, M.; Nasrallah, S. B., On the influence of sodium chloride concentration on equilibrium contact angle. *Chem. Eng. Sci.* **2006,** *122*, (47-53).
67. Johansson.K; Eriksson, J. C., γ and dγ/dT measurements on aqueous solutions of 1,1-electrolytes. *J Colloid Interf Sci* **1974,** *49*, (3), 469-480.
68. Ralston, J.; Healy, T. W., Specific cation effects on water structure at air-water and air-octadecanol, monolayer-water interfaces. *J Colloid Interf Sci* **1973,** *42*, (3), 629-644.
69. Levin, Y.; dos Santos, A. P.; Diehl, A., Ions at the Air-Water Interface: An End to a Hundred-Year-Old Mystery? *Phys. Rev. Lett.* **2009,** *103*, (25), 257802.
70. Marcus, Y., Effect of Ions on the Structure of Water: Structure Making and Breaking. *Chem. Rev.* **2009,** *109*, (3), 1346-1370.
71. Tonnet, N.; Shah, V.; Chiquet, P.; Diaz, J.; Mouronval, G.; Broseta, D. In *Wettability alternation of caprock minerals by acid gases*, Proceedings of the 10th International Symposium on Reservoir Wettability, Abu Dhabi, 26-28 October, 2008.

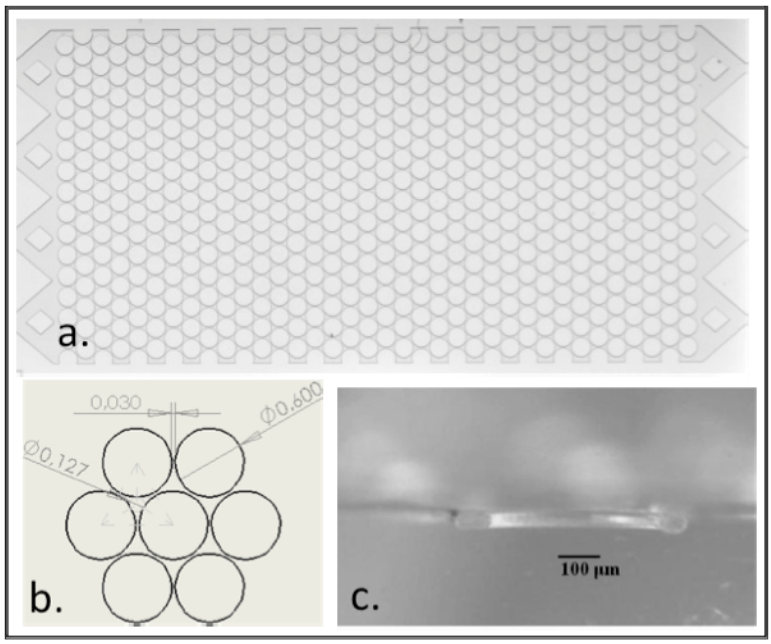

Figure 1. (a) Photograph (plan view) of the micromodel (patterned area 20 mm x 10 mm). (b) Drawing of plan view of pore geometry. (3) Photograph of a cross-section of the pores.

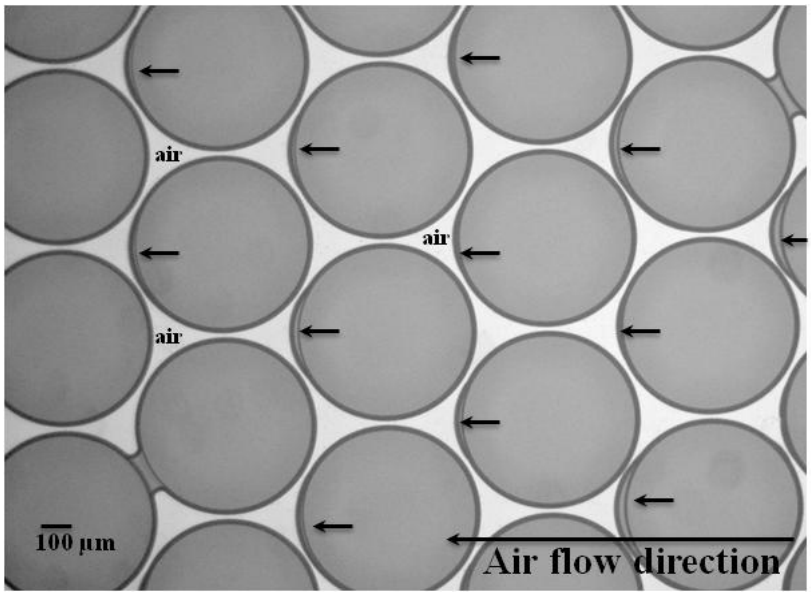

Figure 2. Images of residual water residing as thick water-films coated on the silica grains after air displaced water from the pore space. The dynamic contact angles (measured 11.5˚ ±1.6°) formed by the airflow. Stopping the airflow the advancing contact angles disappeared into the water layer (near zero contact angles under static condition). The silica micromodel is strongly hydrophilic when air is the non-aqueous phase.

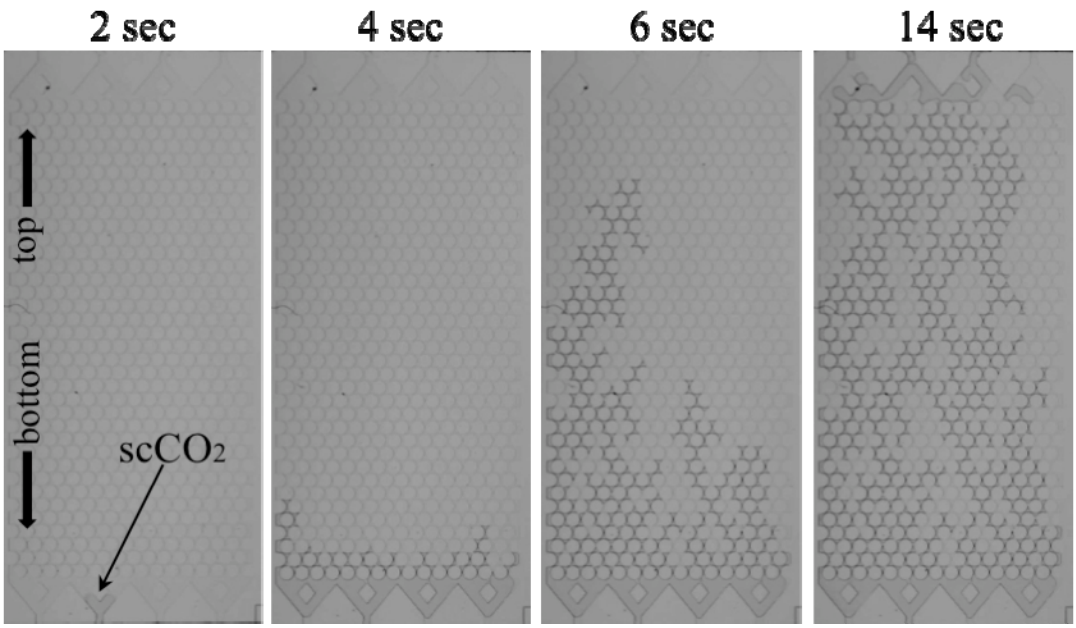

Figure 3. Selected images during drainage process at 8.5 MPa and 45 °C. Supercritical CO_2 was injected at 4 μL/min for 20 min, from the bottom to the top. The pore space was initially saturated with brine (1 M NaCl) then displaced with $scCO_2$. After 100 PV of $scCO_2$ injection, about 85% of the brine was displaced.

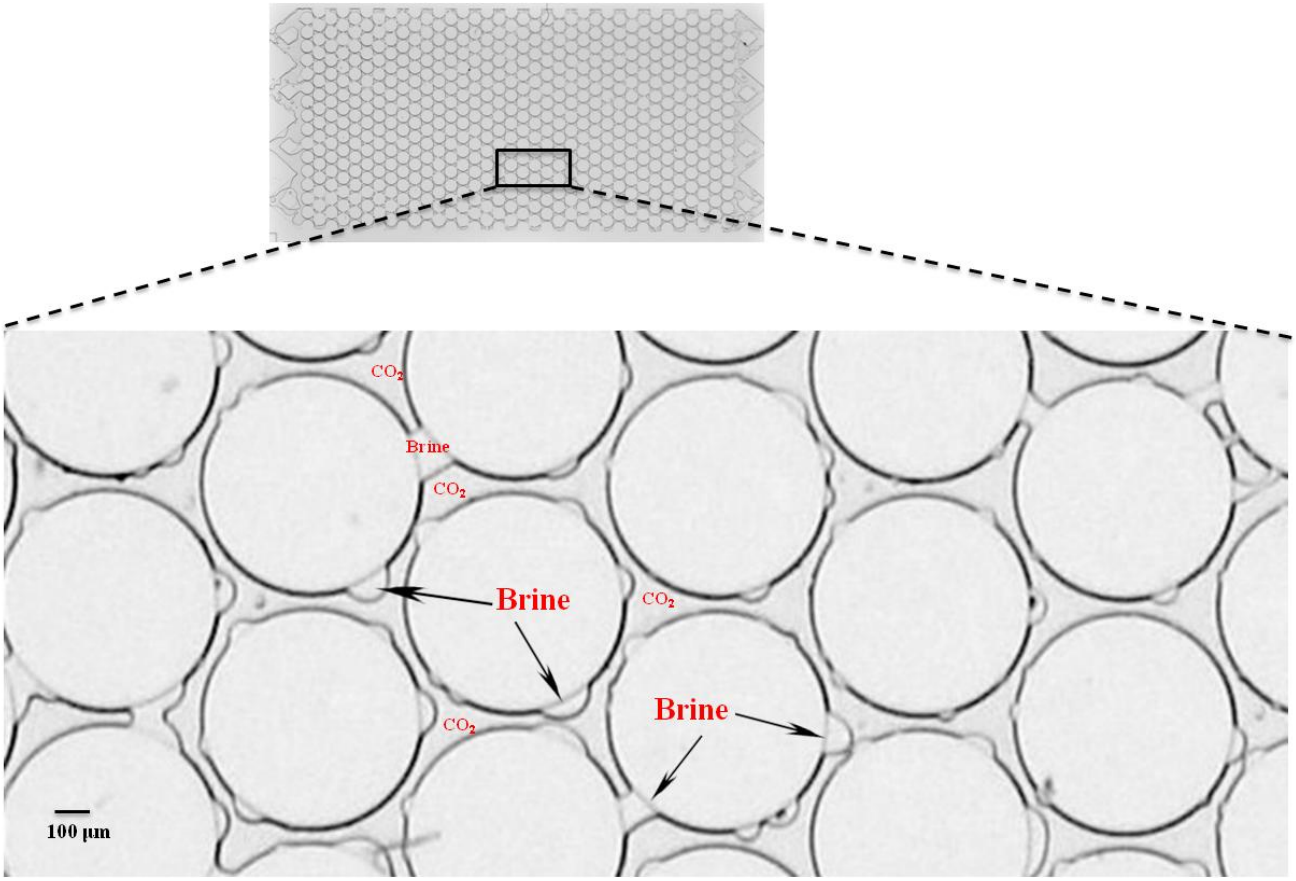

Figure 4. Dewetting of silica surfaces occurred upon reaction with $scCO_2$, shown by formation of water-droplets and increased contact angles. The raw microscope image was taken 2 h after the drainage process at 8.5 MPa and 45 °C with 1 M NaCl brine. The equilibrium contact angles of water-droplets are in the range of 40° to 80°.

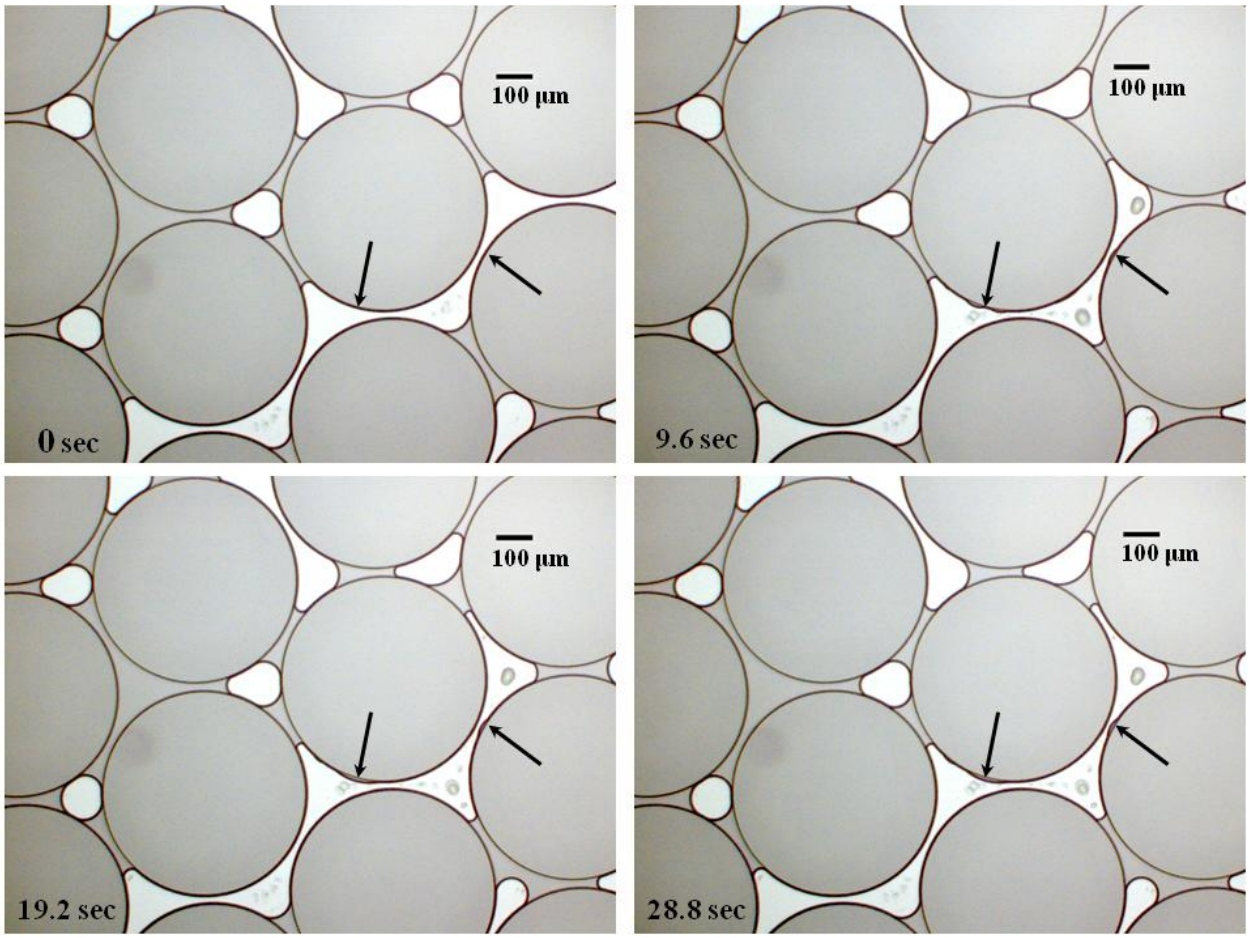

Figure 5. Raw microscope photograph images of the water droplet growth during drainage under conditions of 0.01 M NaCl, 8.5 MPa, and 45 °C. The $scCO_2$ is lighter colored. The water droplets are growing on the silica grains during the drainage (indicated by arrows).

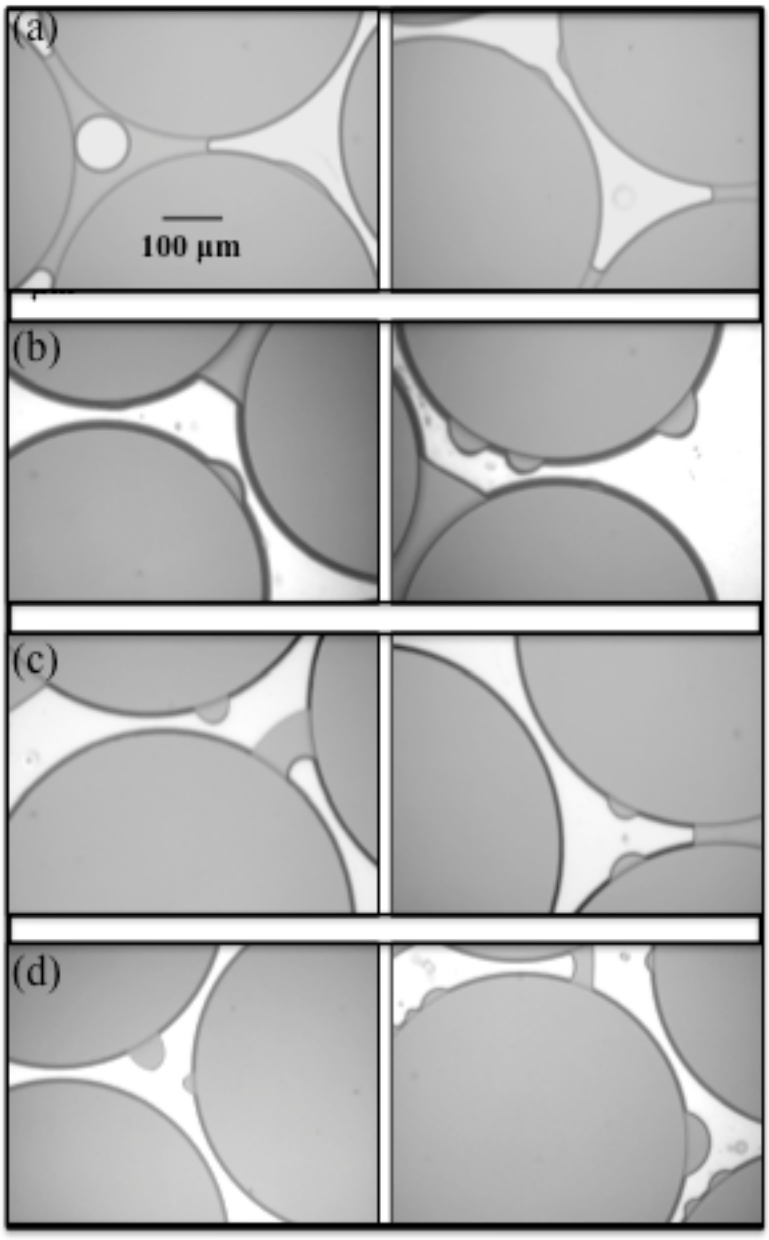

Figure 6. Effect of ionic strength on wetting. The raw microscope images show equilibrium contact angles of water droplets on silica grains after the drainage process at 8.5 MPa and 45 °C. The injected $scCO_2$ is light in color. The NaCl concentrations are (a) 0.01 M; (b) 1 M; (c) 3 M; and (d) 5 M.